Journal of Alloys and Compounds 758 (2018) 5–13

Contents lists available at ScienceDirect

Journal of Alloys and Compounds

journal homepage: http://www.elsevier.com/locate/jalcom

Ultra-thin CoO films grown on different oxide substrates: Size and support effects and chemical stability

D. Díaz-Fernández [a], E. Salas [b], J. Méndez [c], R.J.O. Mossanek [d], M. Abbate [d], C. Morales [a], G. Domínguez-Cañizares [a], G.R. Castro [b], A. Gutiérrez [a], L. Soriano [a, *]

[a] Departamento de Física Aplicada and Instituto de Ciencia de Materiales Nicolás Cabrera, Universidad Autónoma de Madrid, Francisco Tomás y Valiente 7, E-28049, Madrid, Spain
[b] SpLine CRG BM25 Beamline, ESRF, BP 220, 6 rue Jules Horowitz, 38043 Grenoble, France and ICMM-CSIC, Sor Juana Inés de la Cruz 3, E-28049 Madrid, Spain
[c] ESISNA Group, Instituto de Ciencia de Materiales de Madrid, ICMM-CSIC, Sor Juana Inés de la Cruz 3, E-28049 Madrid, Spain
[d] Departamento de Física, Universidade Federal do Paraná, Caixa Postal 19044, 81531-990 Curitiba, PR, Brazil

ARTICLE INFO

Article history:
Received 2 February 2018
Received in revised form
24 April 2018
Accepted 9 May 2018
Available online 10 May 2018

Keywords:
CoO ultra-thin-films
Oxide/oxide interfaces
Chemical stability
Photoemission spectroscopy
Absorption spectroscopy

ABSTRACT

We have studied the growth, interface and chemical stability of ultra-thin CoO films supported on different single crystal oxides as substrates, namely SiO_2, Al_2O_3 and MgO. The films have been grown by reactive evaporation of Co in an oxygen atmosphere at room temperature and analyzed *in situ* by photoemission spectroscopy. Analysis of the Co 2p 3/2 photoemission spectra, supported by theoretical cluster model calculations, reveals size effects for coverages below 5 equivalent monolayers for all substrates. In the case of the Al_2O_3 substrate, the predicted charge transfer from the substrate to the CoO ultra-thin-film has been experimentally observed. The way of growth of the ultra-thin films is dictated by the crystalline structure of each substrate in terms of the lattice mismatch. It has been found that the quality and stability of the films depend more on the structural parameters of the oxide substrates rather than on their covalent/ionic character. The chemical stability of the films upon air exposure and aggressive oxidizing thermal annealing has also been studied. The most suitable substrate to grow ordered and stable CoO ultra-thin-films is MgO whereas nanoclusters of CoO formed at the early stages of growth on SiO_2 appear also to be very stable.

1. Introduction

Cobalt oxides thin films have recently attracted a great interest in materials research due to their unique physical and chemical properties. They find applications as super-capacitors anodes in lithium-ion batteries [1–3], catalyst [4,5], gas sensors [6,7], magnetoresistant [8] and electrochromic [9,10] materials. In particular, CoO is an antiferromagnetic material commonly used in ferromagnetic/antiferromagnetic bilayers for exchange bias devices [11]. All these technological applications involve the growth of CoO layers to make up the corresponding device or coating. The chemical stability of the layer in air conditions and upon thermal annealing is another important aspect for the fabrication of the final device. For instance, it is known that CoO surfaces undergo re-oxidation to Co_3O_4 under air exposure, thus losing their antiferromagnetic properties [12]. The main goal of this paper is a detailed study of the interaction and chemical stability of ultra-thin CoO films grown on different oxides. To this end, we have chosen a set of oxide substrates whose interaction with CoO is relevant in many devices and applications [13–15] and, at the same time, they exhibit very different electronic structure namely, SiO_2, Al_2O_3 and MgO, being SiO_2 predominantly covalent, MgO strongly ionic and Al_2O_3 as intermediate.

We have put special effort in the analysis of the CoO-oxide interface and the chemical stability of the CoO layers. It is known that support, size and other effects may change the final properties of the layer [16,17], in particular for ultra-thin films where these effects are more visible and can be observed at the early stages of the film growth, where the growing material is in direct contact with the support. Interesting trends due to this different covalent-ionic character of the support have been observed at the interfaces formed by these oxides upon deposition of TiO_2 [18–20] and NiO

* Corresponding author.
E-mail address: l.soriano@uam.es (L. Soriano).

https://doi.org/10.1016/j.jallcom.2018.05.112
0925-8388/

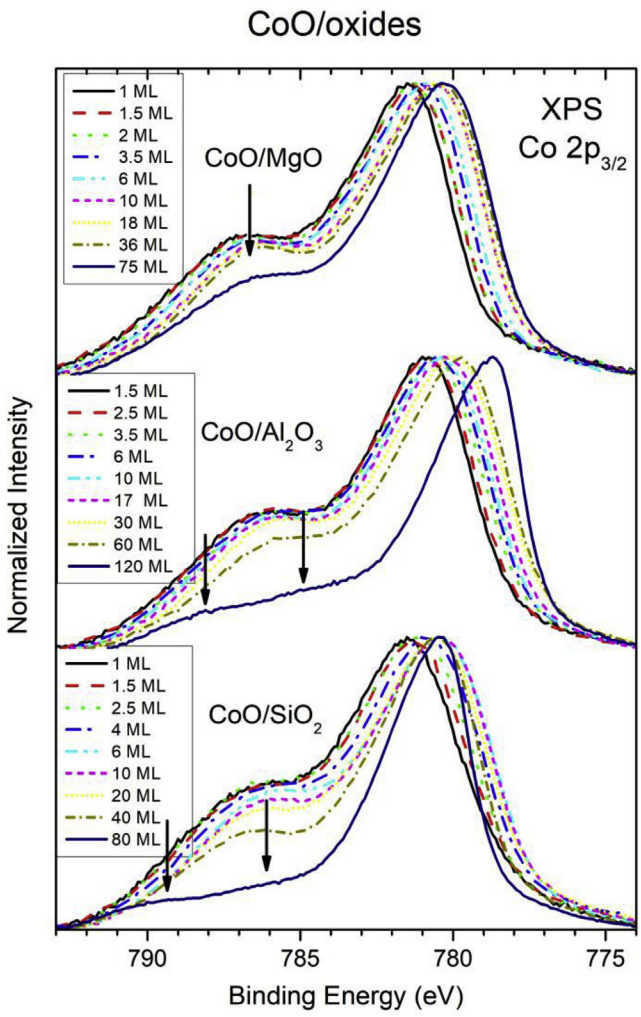

Fig. 1. Co 2p 3/2 XPS spectra of CoO layers on SiO_2 (bottom); Al_2O_3 (center) and MgO (top) for different coverages as labelled.

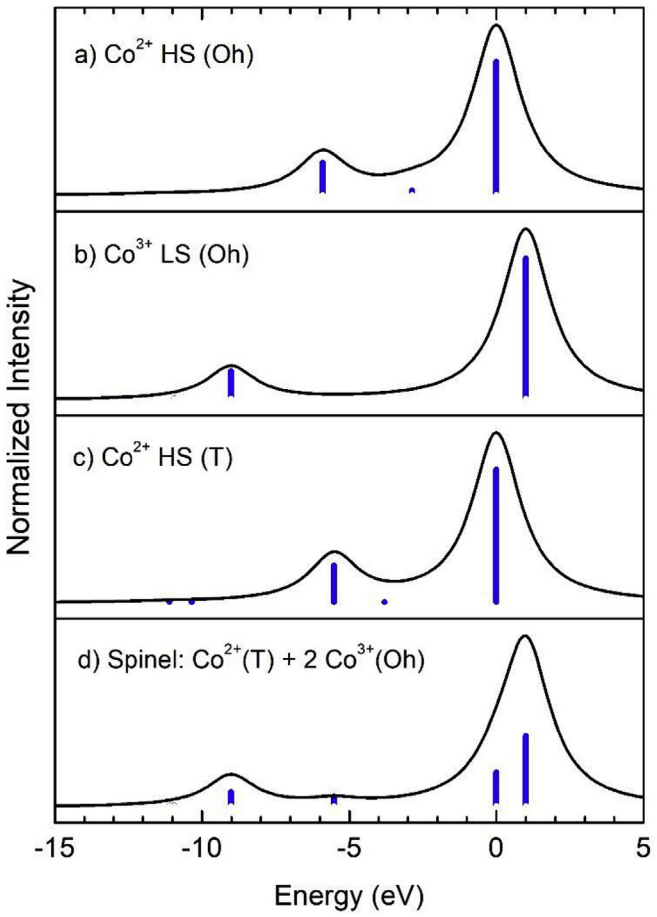

Fig. 2. a) Cluster model calculations of the Co 2p 3/2 XPS peak for different Co ions in different symmetries as labelled.

[21,22].

The early stages of growth of CoO by reactive evaporation on the same set of oxides have already been quantitatively studied by us using XPS and AFM [23]. It was found that the way of growth of CoO on SiO_2 is of Volmer–Weber type (islands growth) whereas the growth on Al_2O_3 and MgO substrates is of Frank-van der Merwe type (layer by layer growth). Other studies dealing with the growth of cobalt oxides on SiO_2 [24] and Al_2O_3 [25] supports have already been reported. In these works, it was found that for polycrystalline SiO_2 substrate, cobalt oxide grows as CoO (Co^{2+}) for reactive oxidation with molecular oxygen gas, whereas for oxidation using oxygen plasma, the spinel Co_3O_4 ($Co^{2+,3+}$) oxide is formed. For the alumina substrate, epitaxial Co_3O_4 films show the formation of fully oxidized interfacial cobalt oxide (Co^{2+}) layer octahedrally coordinated [25].

In this work we have used *in situ* x-ray photoemission (XPS), supported by cluster model calculations, and *ex-situ* x-ray absorption (XANES) spectroscopies to analyze the electronic structure of the ultrathin CoO layers as grown in ultra-high vacuum (UHV) conditions, upon air exposure and upon oxidizing thermal annealing. The morphology of the ultra-thin films formed on the oxide substrates both, before and after annealing, have also been studied by atomic force microscopy (AFM). We first present the XPS results for different stages of the growth of cobalt oxides on the oxide substrates. Then we analyze the experimental Co 2p3/2 XPS spectra in terms of cluster model calculations to obtain information from the interface formed. Finally, results on the chemical stability and morphology of the ultra-thin cobalt oxides layers upon air exposure and thermal annealing for different coverages are presented.

2. Experimental details

Cobalt oxides were grown by reactive thermal evaporation of metallic cobalt in an oxygen atmosphere at 2×10^{-5} mbar. The substrates were single crystals from MTI, with nominal roughness ≤ 5 Å: SiO_2 (x-cut quartz), Al_2O_3 (0001) and MgO (100). The substrates were previously heated at 400 °C in UHV for 60 min to desorb possible contamination and then exposed to oxygen atmosphere at 3×10^{-3} mbar to prevent from oxygen losses. The substrates were at room temperature during evaporation and the evaporation rate was maintained constant and very low (around 0.2 ML/min) to allow the study of the early stages of growth. More details on the quantification of the growth rate can be found elsewhere [23]. The films were grown by successive evaporations and analyzed by XPS after each growth step.

The photoemission spectra were measured with a CLAM-4 MCD hemispherical analyzer spectrometer (Thermo Fisher Scientific) using Al K_α radiation. The pass energy of the analyzer was set to 20 eV, giving an overall resolution of about 1.0 eV. The energy scale was calibrated by adjusting the Si 2p XPS peak for SiO_2 at 103.0 eV

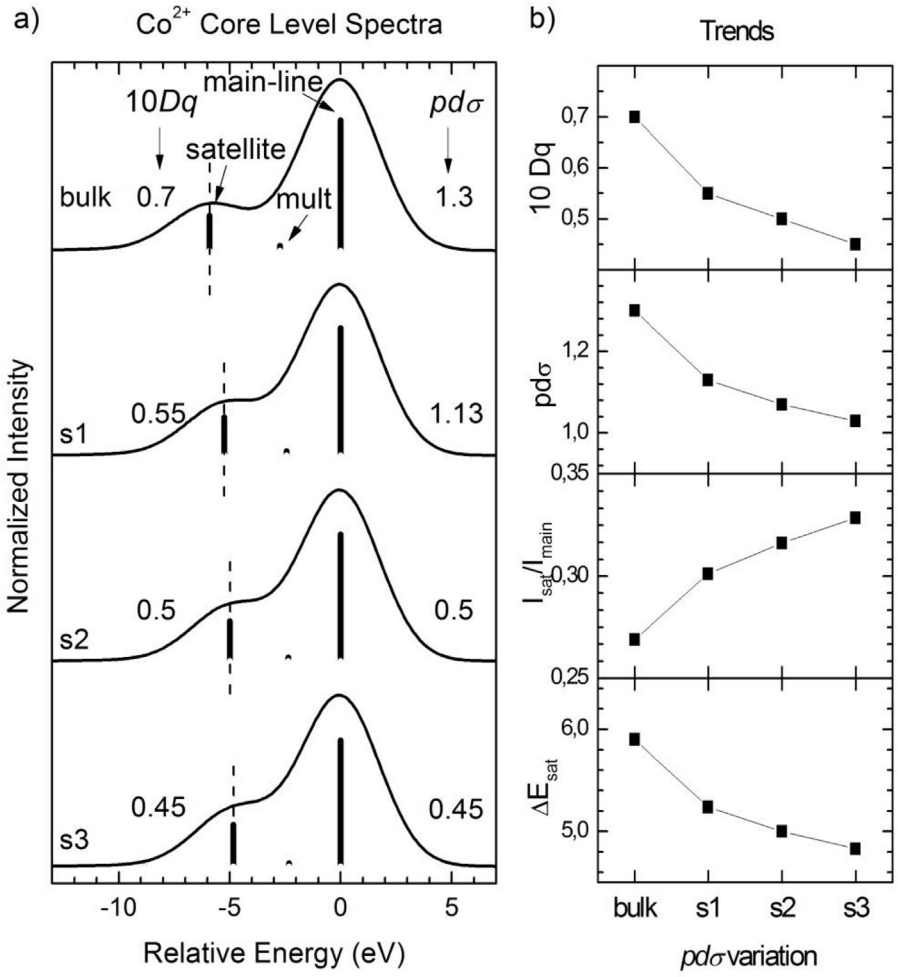

Fig. 3. a) Cluster model calculations of the Co 2p 3/2 XPS peak for different values of the *pdσ* and *10Dq* parameters. b) Main line-satellite energy separation (ΔE_{sat}) and relative intensity (I_{sat}/I_{main}) for the different values of *pdσ* and *10Dq* parameters.

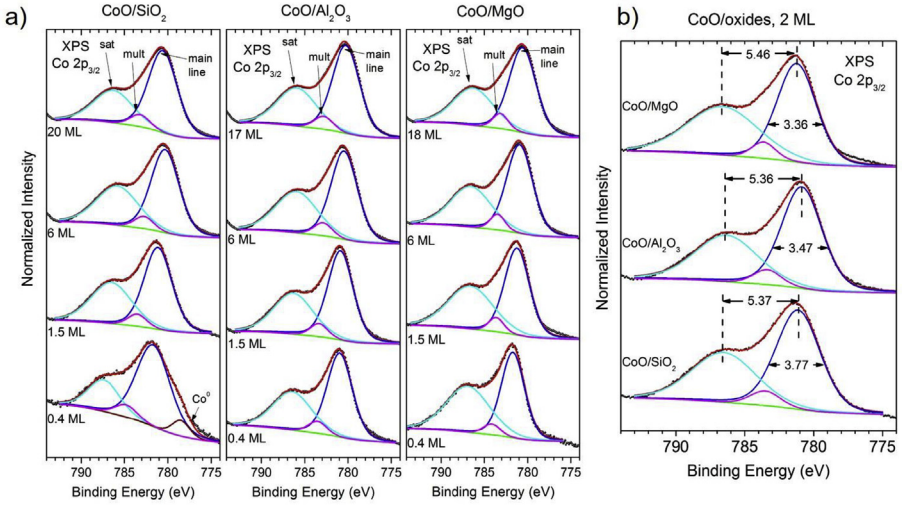

Fig. 4. a) Examples of the fittings performed to the Co 2p 3/2 XPS experimental spectra containing the three peaks given by the calculations of different coverages of CoO grown on the oxide substrates (as labelled). The intensities of the peaks have been left as free parameter. b) The same fittings as before for 2 ML CoO on the substrates. Values for the FWHM of the main line and energy separation are given in eV.

[26], the Al 2p for Al_2O_3 at 74.5 eV [27] and the Mg 2p for MgO at 50.0 eV [28] to correct from possible charging effects. The spectra have been fitted using the XPS Peak software, version 4.1. The Co K ($E \approx 7.76$ keV) x-ray absorption spectra (XAS) were measured *ex-situ* at the SpLine BM25 beamline located at the European Synchrotron Radiation Facility (ESRF) in fluorescence yield mode, using

a multi-element solid-state multichannel detector. The spectra were normalized with the I_0 signal to correct from beam losses. *Ex-situ* AFM images were obtained with a Nanotec AFM microscope in non-contact dynamic (tapping) mode, using commercial tips from Nanosensors. The images were processed and analyzed with the WSxM software [29].

3. Results and discussion

3.1. Growth of cobalt oxides and their interfaces

3.1.1. The XPS spectra

The Co 2p XPS spectra have been measured for each step of growth of the cobalt oxides ultra-thin films on each oxide substrate. As the main changes in the spectra appear at the Co 2p 3/2 XPS peak, we present in Fig. 1 these spectra as a function of the coverage on the three substrates for clarity reasons. The experimental raw Co 2p XPS spectra showing the whole Co 2p doublet are presented in Figs. S1, S2 and S3 as supplementary material of this article. A Shirley background has been subtracted from the experimental spectra and then, they have been normalized for comparison purposes. The coverage is given in equivalent monolayers (ML); more details on the quantification of the coverage of cobalt oxides on the oxide supports can be found elsewhere [23]. At first glance, the spectra obtained for low coverages on all substrates are similar, consisting of a main line about 780 eV binding energy and a satellite at about 786 eV. However, for large coverages (>40 ML), the spectra, especially for SiO_2 and Al_2O_3 substrates, show the main line shifted by c.a. 1 eV with respect to that for low coverages, and a satellite splitting into two weak peaks at c.a. 786 and c.a. 789 eV binding energies. In order to clarify the interpretation of these spectra we present in Fig. 2 theoretical cluster model calculations for different Co ions in different symmetries and configurations. We have used the well known standard parameters given by Bocquet and Fujimori in Ref. [30]. According to these calculations, the spectra for low coverages correspond to Co^{2+} species in octahedral symmetry and high spin configuration (CoO). On the other hand, the spectra for larger coverages approach the calculations for the spinel Co_3O_4 oxide, as they clearly show the splitting of the satellite marked by arrows in Fig. 1. However, the relative intensity of these satellites does not agree with those given by the calculations, since the satellite at c.a. 786 eV, which is due to Co^{2+} species, is much higher in the experimental spectra. This is easily explained by the formation of Co_3O_4 on top of the CoO layer. We want to point out that although for low coverages, CoO grows on all substrates, as expected at room temperature from the Ellingham diagrams shown in Fig. S4 of the supplementary material, for high coverages, Co_3O_4 grows on the previous CoO layer grown on the SiO_2 and Al_2O_3 substrates. Although the energy cost of the formation of Co_3O_4 is larger than for CoO, this can be due to the disorder of the CoO layers grown on these substrates which favours the formation of Co_3O_4. In the case of the spectrum for 75 ML of CoO on the MgO substrate, although the spectrum has shifted toward lower binding energies, the satellite has not diminished to the same extent, as for instance, that of 80 ML on SiO_2, indicating a larger stability of the CoO layer grown on the MgO substrate.

3.1.2. Loss of covalence calculations

CoO is a highly correlated insulator with a gap of 2.5 + 0.3 eV and the first ionization state in CoO corresponds to an intermediate-spin [30]. The analysis of the 2p core-level photoemission peaks of transition metals (TM) in terms of peak-fitting is always a difficult task since many effects like complex multiplet splitting, charge transfer satellites and plasmon loss structures appear in the XPS spectra [31]. However, these structures are very

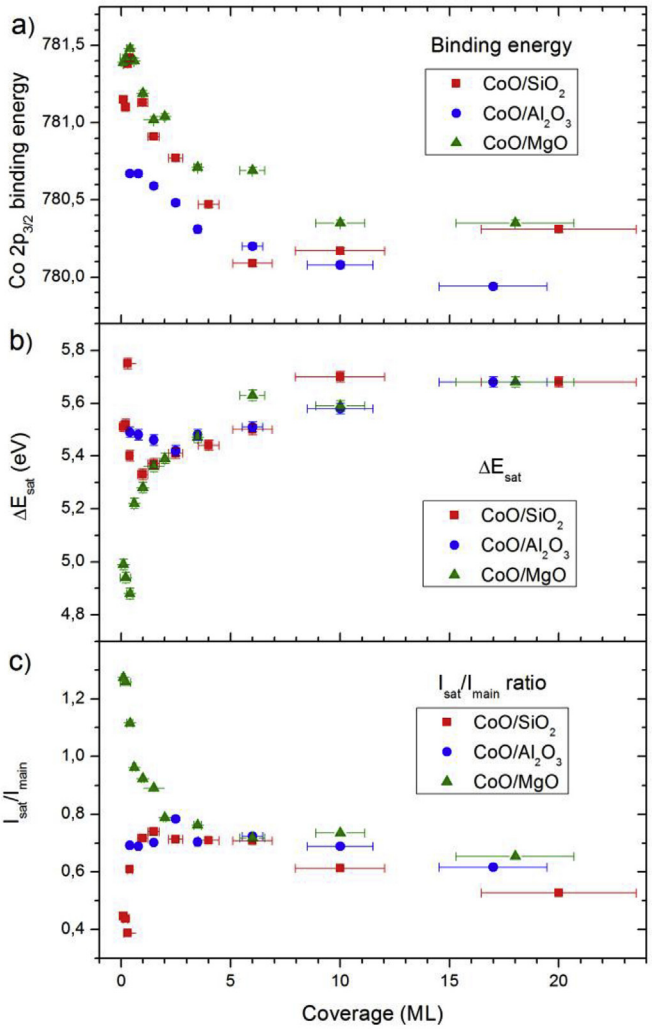

Fig. 5. Results given by the fittings of the Co 2p experimental spectra of CoO on the oxides as a function of the coverage for: a) Co 2p 3/2 main line binding energy position (top panel); b) ΔE_{sat} energy separation (center panel) and c) I_{sat}/I_{main} relative intensity (bottom panel).

sensitive to the local coordination of the TM ions, thus giving valuable information of the system being analyzed. In order to analyze in detail the experimental XPS spectra, we have theoretically calculated the Co 2p XPS spectra by means of cluster model calculations for Co^{2+} ion in octahedral symmetry and high spin configuration. Firstly, the Co 2p XPS peak for a CoO_6 cluster has been calculated using standard parameters [30,32] to account for bulk CoO. Then, the *pdσ* and 10*Dq* parameters, which account for the O 2p-Co 3 d hybridization integral and crystal field respectively, have been intentionally lowered to simulate how a loss of covalence, due for instance to disorder or bi-dimensional effects, affects the relative intensities and energy positions in the experimental spectra. This procedure is similar to the ones developed in studies on the growth of other transition metal oxides [20,21]. The results are shown in Fig. 3a where it is seen that for bulk CoO (top as labelled), the spectrum consists of three different structures labelled as main-line, satellite and multiplet. More details on the electronic structure of this oxide can be found elsewhere [33]. The inferior panels in Fig. 3, labelled as s1, s2 and s3, correspond to the calculations where the *pdσ* and 10*Dq* parameters have been decreased. Fig. 3b shows the values of these parameters in the calculations as well as the energy separation (ΔE_{sat}) of the main-

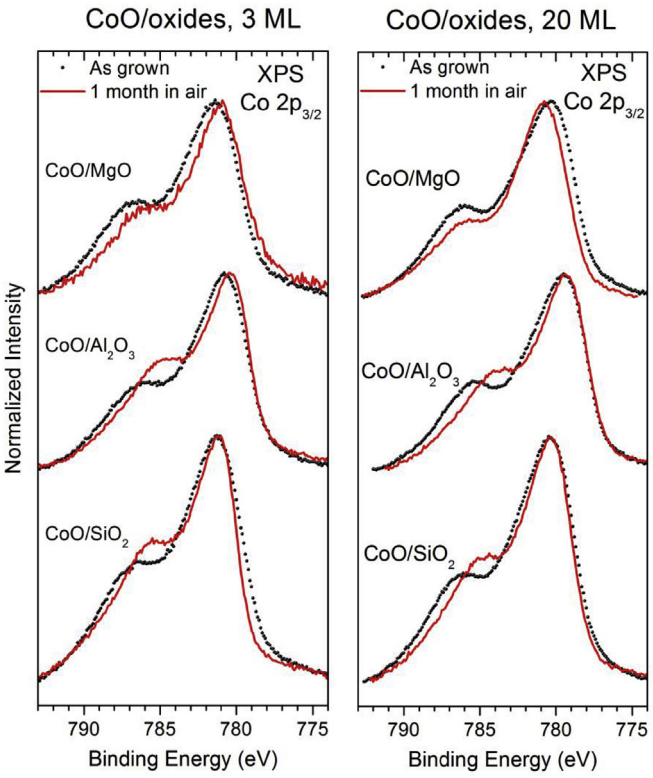

Fig. 6. Co 2p 3/2 XPS spectra of 3 ML and 20 ML of CoO grown on the oxide substrates as grown (dots) and after 1 month exposed to air (lines).

line with respect to the satellite and the main-line/satellite intensity ratio. The results show that as covalence is decreased, ΔE_{sat} diminishes and the relative intensity of the satellite increases. This

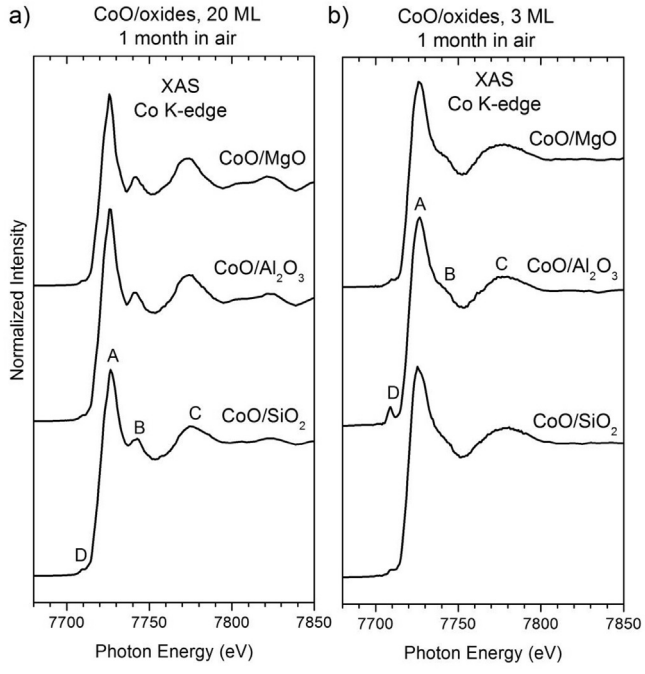

Fig. 7. Co K XAS spectra of: a) 20 ML and b) 3 ML of CoO grown on the oxide substrates (as labelled) after 1 month exposed to air.

means that the larger Co 3 d–O 2p orbital overlap produces the larger energy separation of the main-line and satellite.

According to these calculations we have performed fittings of the Co 2p XPS experimental spectra using the above three structures, whose energy positions and relative intensities have been allowed to vary to obtain the best fittings for the values given by the calculations. Fig. 4 shows, to exemplify our analysis, the fittings performed to the XPS experimental spectra for four different coverages of CoO on the three substrates, showing the background subtraction and the final spectra. In all cases the experimental spectra (dots) are well reproduced showing an excellent agreement with the calculated spectra. Only the spectrum for 0.4 ML of CoO/SiO_2 needs a fourth curve in the fittings to simulate the small amount of metallic cobalt as discussed in Ref. [23].

3.1.3. Analysis of the binding energy shift

As shown in Fig. 1, the binding energy of the main line undergoes continuous shift together with a decrease of the satellite intensity. To analyze these changes, we have depicted in Fig. 5 the results obtained from the fittings of the experimental spectra. In particular, Fig. 5a shows the binding energy of the main line for all the spectra of the samples grown on all oxides. The most significant feature observed is the energy position for all the spectra of the CoO layers grown on Al_2O_3 (circles), which appear shifted to lower binding energies by c.a. 0.7 eV with respect to the spectra of the layers grown on the other oxides. This experimental observation confirms the Density Functional Theory (DFT) calculations performed by Zayed et al. on nanosized CoO films on α- Al_2O_3 (0001) surface [34]. In this work, an electron density transfer of about 0.7 eV from the topmost O layer of the substrate to the first two CoO monolayers is predicted. In this picture, the electric dipole moment created at the interface make photoelectrons gain kinetic energy, thus shifting towards lower binding energies. Apart from this special feature for the Al_2O_3 substrate, the spectra for all substrates undergo continuous shifts as the coverage increases, especially for very low coverages under 10 ML. This shift can be interpreted as due to quantum-size effects. Indeed, it is known that when the dimension of a nanostructure approaches the atomic scale in nanoparticles or nanofilms, the photoemission spectra moves towards higher binding energies. This has been observed in CuO nanoparticles [35] and TiO_2 ultra-thin films [36]. In our case, this effect is observed for all oxide supports for coverages below 5 ML i.e. about 1 nm. However, we want to point out that in the case of the SiO_2 substrate, CoO grows forming small clusters or nanoparticles for coverages below 4–5 ML (equivalent) whereas for the Al_2O_3 and MgO substrates CoO grow in a layer by layer mode as it is shown in Ref. [23]. In any case, we can conclude that size effects are clearly observed in both, CoO nanoparticles and ultra-thin films, formed at the early stages of growth on these oxides. For larger coverages, the binding energy of the main-line approaches the value for bulk CoO indicating that a stoichiometric CoO thin film has been formed on all substrates.

3.1.4. Analysis of the effect of the support

As mentioned above, the oxides used as substrates in this work differ in their electronic structure, in particular in the covalent-ionic character of their O-metal bonds. We have already observed interesting interfacial effects by deposition of TiO_2 and NiO layers [20,21] on the above oxide substrates. For these TM oxides, the strong covalent character of the Si–O bonding in SiO_2 weakens the covalence of the overlayers as observed by the Ti 2p absorption and Ni 2p photoemission spectra respectively. As the covalent character of the oxide substrate decreases (SiO_2>Al_2O_3>MgO), such reduction is less important.

In the case of CoO, cluster model calculations of the Co 2p XPS

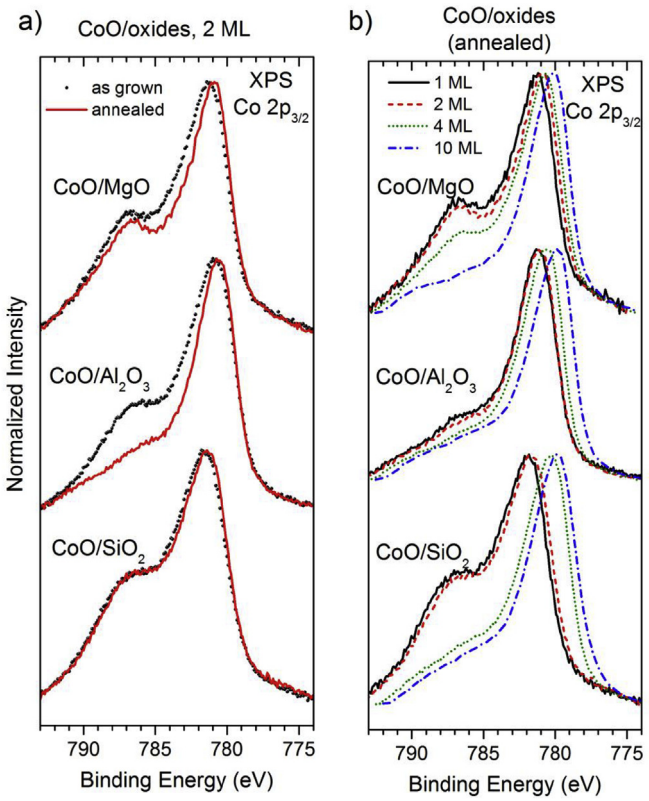

Fig. 8. Co 2p 3/2 XPS spectra of: a) 2 ML of CoO on the oxide substrates (as labelled) and b) 1, 2, 4 and 20 ML of CoO on the oxide substrates (as labelled) as grown (solid line) and after annealing (lines as indicated).

spectra have shown that the loss of covalence (by diminishing the *pdσ* and *10Dq* parameters) produces a decrease of the main-line to satellite energy separation (ΔE_{sat}). To investigate this effect in our samples, we have depicted in Fig. 5b ΔE_{sat} versus coverage for the CoO layers on the three oxides. Surprisingly, for coverages <4 ML, the ΔE_{sat} values are larger for the SiO_2 substrate than for the more ionic MgO substrate, just the contrary as it was expected in comparison to NiO oxide as already discussed [21]. Also the relative intensity ratio of the satellite and main line I_S/I_M data presented in Fig. 5c confirms the above conclusions. The intensity of the satellite is higher in the spectra of the CoO layers grown on the MgO substrate than those of the others, whereas it is significantly lower for those grown on SiO_2.

According to the experimental results obtained above, it seems that in the case of the CoO oxide, the covalence-ionicity of the substrate does not affect the electronic structure of the early stages of growth of the CoO overlayers. However, the FWHM values given in Fig. 4b for the main line are narrower for MgO than for SiO_2. This behavior suggests the growth of a more ordered CoO layer on MgO than on SiO_2 which, on the other hand, is not surprising taking into account the better matching of the lattice parameter of CoO (a = 4.26 Å) with that of MgO (a = 4.21 Å) than with those of Al_2O_3 (a = 4.76 Å) and SiO_2 (a = 4.91 Å). Besides, Co atoms have an octahedral coordination in CoO, the same as Al atoms in Al_2O_3 and Mg atoms in MgO whereas Si atoms have a tetrahedral coordination in SiO_2. This suggests to be also the reason why CoO grows in a layer by layer mode on Al_2O_3 and MgO whereas for SiO_2 it grows forming nanometric islands. In summary we can conclude that the effect of the substrate for the growth of CoO is more related to the structural properties of the oxide substrates than to their electronic structure in terms of covalence/ionicity.

3.2. Chemical stability upon air exposure

One of the main goals of this work is the study of the chemical stability of the ultra-thin CoO layers upon air exposure. For this purpose, we have measured the XPS spectra of samples containing 3 and 20 ML of CoO grown on the different oxide substrates after 1 month exposed to air. Fig. 6 shows the Co 2p 3/2 XPS spectra for those samples as grown and after air exposure. Although all the initial spectra show small changes upon air exposure, the films grown on MgO show less changes, conserving the initial ΔE_{sat} energy separation and the relative intensity of the satellite. However, the spectra for the CoO films grown on Al_2O_3 and SiO_2 substrates show a clear increase of the intensity of the satellite and a decrease the energy separation ΔE_{sat}. According to the above calculations, this effects are consistent with a slight loss of covalence due to air contamination probably due to the presence of uncoordinated Co atoms. In general, all the spectra resemble that of CoO (Co^{2+}) and are far away from the spectra of Co_3O_4 ($Co^{2+,3+}$) for which the intensity of the satellite are much lower with the presence of a second satellite at higher binding energies. These results suggest that the CoO layers on the MgO substrate are more stable upon air exposure than those grown on Al_2O_3 and SiO_2 substrates, which seem to be more sensitive to atmosphere contamination.

We have also measured the XAS spectra at the Co K absorption edge in fluorescence yield for samples containing 3 ML and 20 ML on all substrates after 1 month exposed to air, as shown in Fig. 7. The spectra are related to the unoccupied electronic states at the conduction band and are site selective and very sensitive to the local symmetry [37]. First of all, we have to point out that the mean probing depth in fluorescence yield for XAS is much larger (several microns) than for XPS (20 Å), so that the spectra should reflect the bulk properties of the analyzed material with minor contribution of the surface contamination. In general, the spectra for 20 ML CoO on the oxide substrates (Fig. 7a) consist of a high peak at the edge threshold about 7730 eV (labelled as A) and two more resonant structures at 7740 eV and 7770 eV (labelled as B and C). Also a small pre-peak at 7710 is observed (labelled as D). All the spectra are almost identical and match other spectra published elsewhere for CoO [38]. Fig. 7b shows the Co K XAS spectra for 3 ML CoO on the oxides. Although the spectra are similar to those for 20 ML, showing the same set of structures A, B, and C, in this case these structures are much broader and less defined. These broadening effects are attributed to the low dimensionality of the analyzed material. Indeed, this effect has also been observed by us in NiO [22] where, according to the multiple scattering theory developed by Benfatto et al. [39,40], the spectra of 80 ML of NiO grown on the same oxides was accurately simulated using a 93 atoms cluster whereas the best simulation for the spectra of 3 ML of NiO used only 19 atoms. Nevertheless, the most interesting difference between the spectra shown in Fig. 7b is the high intensity of the pre-peak of the spectrum for the Al_2O_3 substrate. This increase in intensity of the pre-peak has been assigned in the literature to Co atoms tetrahedrally coordinated [41,42] in the spectra for $CoAl_2O_4$. According to this, XAS seems to indicate the formation of $CoAl_2O_4$ at the CoO/Al_2O_3 interface. It is important to note that Co atoms in both, Al_2O_3 and $CoAl_2O_4$, are in the form of Co^{2+}, so that the XPS spectra have been only able to observe the oxidation state of the cobalt atoms whereas the high sensitivity to the local symmetry of XAS has allowed to detect the formation of the binary oxide at the CoO/Al_2O_3 interface. These conclusions are also supported by the strong diffusion of Co atoms into well ordered Al_2O_3 upon thermal annealing reported in Refs. [43,44]. Therefore, we can conclude that air exposure does not

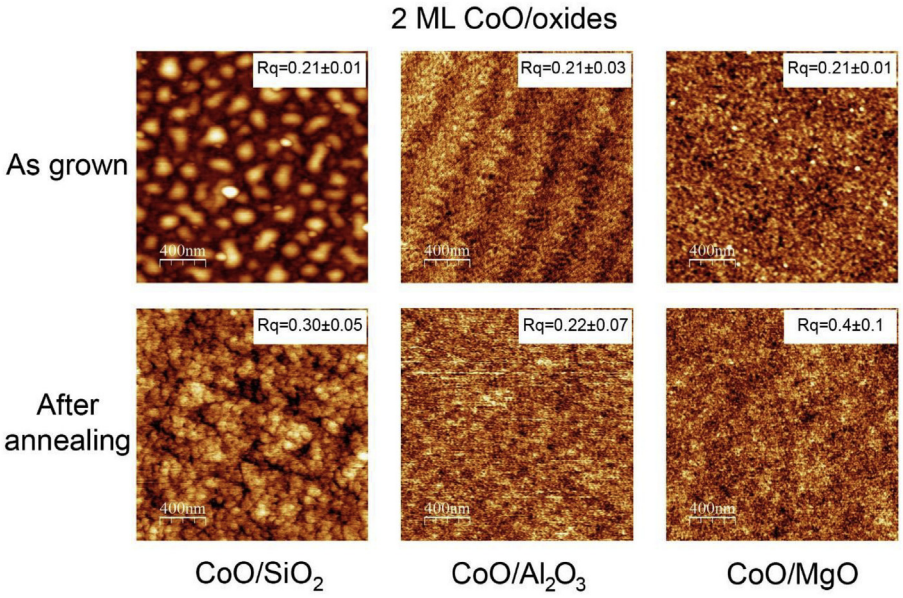

Fig. 9. $2 \times 2\,\mu m^2$ AFM images of 2 ML of CoO as grown (top) and after annealing (bottom) on the oxide substrates (as labelled).

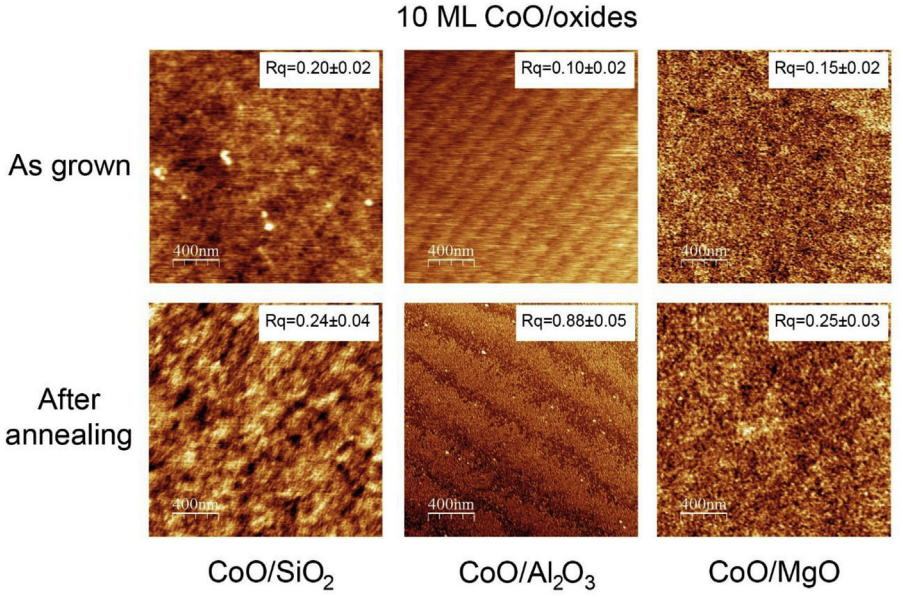

Fig. 10. $2 \times 2\,\mu m^2$ AFM images of 10 ML of CoO as grown (top) and after annealing (bottom) on the oxide substrates (as labelled).

affect the octahedrally coordinated CoO grown on the SiO_2 and MgO substrates, however it promotes the formation of $CoAl_2O_4$ at the CoO/Al_2O_3 interface.

3.3. Chemical stability upon oxidizing thermal annealing

In this section we study the stability behavior of the CoO layers upon a more oxidizing process. To this end, samples with different coverages have been submitted to thermal annealing at 400 °C in an oxygen atmosphere of 1×10^{-3} mbar. The Co 2p 3/2 XPS spectra for 2 ML of CoO/grown on the different oxide substrates, before (dots) and after (lines) annealing are depicted in Fig. 8a. The spectra corresponding to the SiO_2 and MgO substrates almost do not change upon annealing however the spectrum for the Al_2O_3 substrate clearly changes severely, suggesting oxidation to Co_3O_4 as observed in the significant loss of intensity of the satellite. Films with different thickness containing 1, 2, 4 and 10 CoO ML on each of the oxide substrates were also submitted to the same annealing. Their Co 2p 3/2 XPS spectra are shown in Fig. 8b. For coverages of 10 ML the CoO layers on all the oxides undergo oxidation to Co_3O_4 as it is inferred from the shape of the spectra. In particular, all the CoO layers grown on the Al_2O_3 substrate always oxidize to the spinel oxide independently of the coverage. In turn, the spectra for coverages of 1 and 2 ML of CoO on the SiO_2 and MgO substrates remain unchanged with respect to the as grown spectra, indicating a great stability upon annealing.

In summary we have found that Al_2O_3 is the less stable substrate to obtain stable CoO layers. The formation of the binary $CoAl_2O_4$ oxide, probably induced by the charge transfer from the substrate to the CoO layer, seems to be responsible of such instability. On the

other hand, 2 ML of CoO on SiO_2 in the form of small nanoparticles, seem to be very stable up to coalescence (<2 ML). Further coverages produce the oxidation of the CoO layer. Finally, the CoO layers grown on MgO appear to be the most stable films although they also get oxidized at higher coverages (<4 ML).

An interesting aspect of these experiments is to compare the morphology of the CoO layers before and after annealing. Figs. 9 and 10 show the $2 \times 2\ \mu m^2$ AFM images of samples containing 2 ML and 10 ML respectively of CoO on the oxides substrates, before (top) and after (bottom) annealing. The mean square roughness calculated by flood analysis is given for each image. As already indicated, CoO on the SiO_2 substrate forms nanoparticles (150–250 nm) rather than homogeneous layers, as observed in Fig. 9 (top-left). Upon annealing, these CoO nanoparticles reduce their size (70–160 nm) but still conserve their morphology as nanoparticles as shown in Fig. 9 (bottom-left). These results indicate that when CoO is in the form of nanoparticles deposited on the SiO_2 substrate, these nanoparticles are chemically stable upon annealing. In turn, when coalescence is produced at coverages >2 ML and CoO forms a continuous layer, as in the case of 10 ML on SiO_2 (Fig. 10 top-left), the CoO layer becomes unstable and undergo re-oxidation to Co_3O_4 (see also Fig. 8b). This seems to be related to the high surface energy of CoO and Co_3O_4 nanoparticles as discussed in Ref. [45]. The images for the as grown 2 and 10 ML of CoO on the alumina substrate (Figs. 8 and 9 top-center) show the typical terraces of the Al_2O_3 single crystal surface, as corresponds to a layer-by-layer way of growth [23]. It is seen that upon annealing, the morphology of these samples almost do not change, still showing the terraces of the substrate, although we have already seen that are chemically different. Finally, the images for 2 and 10 ML of CoO grown on MgO (Figs. 8 and 9 top-right) show no island formation. They do not change upon annealing giving also a very low roughness.

4. Conclusions

We have studied the growth and chemical stability of ultra-thin cobalt oxide layers deposited on oxides substrates with different covalent/ionic ratio: SiO_2, Al_2O_3 and MgO. As deduced from the XPS chemical shift observed in the Co 2p 3/2 spectra, we have found an experimental evidence of the charge transfer produced at the CoO/Al_2O_3 interface as predicted by DFT. For CoO coverages below 5 ML, size effects have been observed in all substrates, in agreement with other published works. The effect of the electronic structure of the substrates, i.e. covalent-ionic character of their bonds, does not seem to play a relevant role in the electronic structure properties of the CoO layers, however the structural parameters of the substrates, like lattice parameter, dictate both, the way of growth of CoO and its chemical stability. MgO has been found to be the most suitable substrate to obtain ordered CoO layers by reactive evaporation in UHV. Exposure to air of the grown CoO layers produce the formation of $CoAl_3O_4$ at the CoO/Al_2O_3 interface whereas CoO remains stable on the other substrates. This different behavior for the alumina substrate seems to be related to the charge transfer occurred at the interface. Aggressive oxidizing annealing of the layers does not produce significant changes in the original morphology of the deposits (nanoparticles for SiO_2, and ordered layers for Al_2O_3 and MgO). However, it produces re-oxidation for any coverage on Al_2O_3. For the SiO_2 substrate, CoO is stable while it grows as nanoparticles up to coverages of ≈2 ML. Once coalescence is produced, the nanostructured ultra-thin-film undergoes re-oxidation to the spinel Co_3O_4 oxide. MgO is the best substrate to obtain chemically and structurally stable CoO layers up to 4 ML. Both, the formation of stable CoO particles on the SiO_2 substrate and ordered layers on MgO up to 2 ML seems to be an important issue in magnetic devices fabrication.

Acknowledgments

This investigation has been funded by the MINECO of Spain through the FIS2015-67367-C2-1-P project and by the Comunidad de Madrid through the NANOFRONTMAG-CM P2013/MIT2850 project. Authors R.J.O.M and M.A. thank the financial support of Conselho Nacional de Desenvolvimento Científico e Tecnológico (CNPq-Brazil). We acknowledge MINECO and CSIC for financial support and provision of synchrotron radiation and we would like to thank the staff of SpLine at ESRF. One of the authors (C.M.) thanks MECD for a FPU grant.

Appendix A. Supplementary data

Supplementary data related to this article can be found at https://doi.org/10.1016/j.jallcom.2018.05.112.

References

[1] X.-C. Dong, H. Xu, X.-W. Wang, Y.-X. Huang, M.B. Chan-Park, H. Zhang, L.-H. Wang, ACS Nano 6 (2012) 3206.
[2] T.-Y. Wei, C.-H. Chen, K.-H. Chang, S.-Y. Lu, C.-C. Hu, Chem. Mater. 21 (2009) 3228.
[3] Z.-S. Wu, W. Ren, L. Wen, L. Gao, J. Zhao, Z. Chen, G. Zhou, F. Li, H.-M. Cheng, ACS Nano 4 (2010) 3187.
[4] F. Jiao, H. Frei, Angew. Chem. Int. Ed. 48 (2009) 1841.
[5] Y. Liang, Y. Li, H. Wang, J. Zhou, J. Wang, T. Regier, H. Dai, Nat. Mater. (2011) 780.
[6] J. Park, X. Shen, G. Wang, Sensor. Actuator. B Chem. 136 (2009) 494.
[7] J. Yang, W.-D. Zhang, S. Gunasekaran, Electrochim. Acta 56 (2011) 5538.
[8] H. Xing, W. Kong, C. Kim, S. Peng, S. Sun, Z. Xu, H. Zeng, J. Appl. Phys. 105 (2009), 063920.
[9] X.H. Xia, J.P. Tu, J. Zhang, J.Y. Xiang, X.L. Wang, X.B. Zhao, ACS Appl. Mater. Interfaces 2 (2010) 186.
[10] X.H. Xia, J.P. Tu, J. Zhang, J.Y. Xiang, X.L. Wang, X.B. Zhao, Sol. Energy Mater. Sol. Cells 94 (2010) 386.
[11] B. Beschoten, J. Keller, P. Miltényi, G. Güntherodt, J. Magn. Magn Mater. 240 (2002) 248.
[12] P. Miltényi, M. Gierlings, J. Keller, B. Beschoten, G. Güntherodt, U. Nowak, K.D. Usadel, Phys. Rev. Lett. 84 (2000) 4224.
[13] N. Koshizaki, K. Yasumoto, S.-Ya Terauchi, Jpn. J. Appl. Phys. 34 (34–1) (1995) 119.
[14] J.R. Taylor, V.J. Wall, M.I. Pownceby, Am. Mineral. 77 (1992) 284.
[15] A. Lyngfelt, B. Leckner, T. Mattisson, Chem. Eng. Sci. 56 (2001) 3101.
[16] V.E. Henrich, Prog. Surf. Sci. 50 (1995) 77.
[17] V.E. Henrich, P.A. Cox, in: The Surface Science of Metal Oxides, Cambridge University Press, Cambridge, 1994. Chap. 7.
[18] L. Soriano, G.G. Fuentes, C. Quirós, J.F. Trigo, J.M. Sanz, P.R. Bressler, A.R. González-Elipe, Langmuir 16 (2000) 7066.
[19] M. Sánchez-Agudo, L. Soriano, C. Quirós, J. Avila, J.M. Sanz, Surf. Sci. 482/485 (2001) 470.
[20] L. Soriano, M. Sánchez-Agudo, R.J.O. Mossanek, M. Abbate, G.G. Fuentes, P.R. Bressler, L. Alvarez, J. Méndez, A. Gutiérrez, J.M. Sanz, Surf. Sci. 605 (2011) 539.
[21] I. Preda, A. Gutiérrez, M. Abbate, F. Yubero, J. Méndez, L. Alvarez, L. Soriano, Phys. Rev. B 77 (2008) 075411.
[22] I. Preda, L. Soriano, D. Díaz-Fernández, G. Domínguez-Cañizares, A. Gutiérrez, G.R. Castro, J. Chaboy, J. Synchrotron Radiat. 20 (2013) 635.
[23] D. Díaz-Fernández, J. Méndez, F. Yubero, G. Domínguez-Cañizares, A. Gutiérrez, L. Soriano, Surf. Interface Anal. 46 (2014) 975.
[24] V.M. Jiménez, J.P. Espinós, A.R. González-Elipe, Surf. Interface Anal. 26 (1998) 62.
[25] C.A.F. Vaz, D. Prabhakaran, E.I. Altman, V.E. Henrich, Phys. Rev. B 80 (2009), 155457.
[26] J.F. Moulder, W.F. Stickle, P.E. Sobol, K.D. Bomben, in: Jill Chastain (Ed.), Handbook of X-ray Photoelectron Spectroscopy, Perkin-Elmer Corporation, 1992. ISBN: 0855012080.
[27] E. Paparazzo, in: Surface and Interface Analysis, vol. 12, 1988, p. 115.
[28] R. Hoogewijs, L. Fiermans, J. Vennik, J. Electron. Spectrosc. Relat. Phenom. 11 (1977) 171.
[29] I. Horcas, R. Fernández, J.M. Gómez Rodríguez, J. Colchero, J. Gómez Herrero, A.M. Baró, Rev. Sci. Instrum. 78 (2007) 013705.
[30] A.E. Bocquet, T. Mizokawa, T. Saitoh, H. Namatame, A. Fujimori, Phys. Rev. B 46 (1992) 3771.
[31] M.C. Biesinger, B.P. Payne, A.P. Grosvenor, L.W.M. Lau, A.R. Gerson, R.StC. Smart, Appl. Surf. Sci. 257 (2011) 2717.

[32] G. van der Laan, C. Westra, C. Haas, G.A. Sawatzky, Phys. Rev. B 23 (1981) 4369.
[33] J. van Elp, J.L. Wieland, H. Eskes, P. Kuiper, G.A. Sawatzky, Phys. Rev. B 44 (1991) 6090.
[34] A. Zayed, A.M. Márquez, J.F. Sanz, J. Phys. Chem. C 117 (2013) 22714.
[35] K. Borgohain, J.B. Singh, M.V. Rama Rao, T. Shripathi, S. Mahamuni, Phys. Rev. B 61 (2000) 11093.
[36] J.P. Espinós, G. Lassaletta, A. Caballero, A. Fernández, A.R. González-Elipe, A. Stampfl, C. Morant, J.M. Sanz, Langmuir 14 (1998) 4908.
[37] J.C. Fuggle, J. Englesfield (Eds.), Unoccupied Electronic States: Fundamentals for Xanes, Eels, Ips and Bis (Topics in Applied Physics), Springer-Verlag, 1992.
[38] T. Jiang, D.E. Ellis, J. Mater. Res. 11 (1996) 2242.
[39] M. Benfatto, S. Della Longa, J. Synchrotron Radiat. 8 (2001) 1087.
[40] M. Benfatto, J.A. Solera, J. Chaboy, M.G. Proietti, J. García, Phys. Rev. B 56 (1997) 2447.
[41] A.M. Beale, G. Sankar, Chem. Mater. 18 (2006) 263.
[42] M.O. Figueiredo, T.P. Silva, J.P. Veiga, J. Electron. Spectrosc. Relat. Phenom. 185 (2012) 97.
[43] M. Heemeier, S. Stempel, ShK. Shaikhutdinov, J. Libuda, M. Bäumer, R.J. Oldman, S.D. Jackson, H.-J. Freund, Surf. Sci. 523 (2003) 103.
[44] M. Raïssi, S. Vizzini, G. Langer, N. Rochdi, H. Oughaddou, C. Coudreau, S. Nitsche, F. Arnaud D'Avitaya, B. Aufray, J.-L. Lazzari, Thin Solid Films 42 (2010) 5992.
[45] L. Wang, K. Vu, A. Navrotsky, R. Stevens, B.F. Woodfield, J. Boerio-Goates, Chem. Mater. 16 (2004) 5394.